

# Molecular Insights into the Metal Selectivity of the Copper(I)-Sensing Repressor CsoR from *Bacillus subtilis*<sup>†</sup>

Zhen Ma,<sup>‡,§</sup> Darin M. Cowart,<sup>||</sup> Robert A. Scott,<sup>||</sup> and David P. Giedroc<sup>\*,‡</sup>

Department of Chemistry, Indiana University, Bloomington, Indiana 47405-7102, Department of Biochemistry and Biophysics, Texas A&M University, College Station, Texas 77843-2128, and Departments of Chemistry, Biochemistry, and Molecular Biology, University of Georgia, Athens, Georgia 30602

Received January 25, 2009; Revised Manuscript Received February 26, 2009

**ABSTRACT:** *Bacillus subtilis* CsoR (*Bsu* CsoR) is a copper-sensing transcriptional repressor that regulates the expression of the *copZA* operon encoding a copper chaperone and a Cu efflux P-type ATPase, respectively. *Bsu* CsoR is a homologue of *Mycobacterium tuberculosis* CsoR (*Mtb* CsoR), representative of a large Cu(I)-sensing regulatory protein family. We show here that *Bsu* CsoR binds  $\approx 1$  mol equiv of Cu(I) per monomer in vitro with an affinity  $\geq 10^{21}$  M<sup>-1</sup>. X-ray absorption spectroscopy shows Cu(I) adopts a trigonal S<sub>2</sub>N coordination like *Mtb* CsoR. Both apo and Cu(I)-bound *Bsu* CsoR are stable tetramers in the low micromolar monomer concentration range by sedimentation velocity and equilibrium ultracentrifugation. Apo-*Bsu* CsoR binds to a pseudopalindromic 30 bp *copZA* operator–promoter DNA with a stoichiometry of two tetramers per DNA and stepwise affinities of  $K_1^{\text{apo}} = 3.1(\pm 0.8) \times 10^7$  M<sup>-1</sup> and  $K_2^{\text{apo}} = 8.3(\pm 2.2) \times 10^7$  M<sup>-1</sup> (0.4 M NaCl, 25 °C, pH 6.5). Cu(I) *Bsu* CsoR binds to the same DNA with greatly reduced affinities,  $K_1^{\text{Cu}} = 2.9(\pm 0.4) \times 10^6$  M<sup>-1</sup> and  $K_2^{\text{Cu}} \leq 1.0 \times 10^5$  M<sup>-1</sup> consistent with a copper-dependent derepression model. This Cu-dependent regulation is abrogated by a “second shell” Glu90-to-Ala substitution. *Bsu* CsoR binds Ni(II) with very high affinity but forms a non-native coordination geometry, as does Co(II) and likely Zn(II); none of these metals strongly regulates *copZA* operator DNA binding in vitro. The implications of these findings on the specificity of metal-sensing sites in CsoR/RcnR proteins are discussed.

As an essential catalytic cofactor of metalloenzymes, copper (Cu) plays crucial roles in many important biological processes (1). The reversible oxidation of Cu(I) and reduction of Cu(II) makes Cu versatile in catalyzing a wide range of different chemical reactions in the cell. However, these redox properties also make Cu toxic with the amounts of “free” Cu inside the cell thought to be strongly limiting. An undesirable pool of available Cu in the cytosol could mediate the production of reactive oxygen species (ROS), i.e., OH<sup>•</sup> and O<sub>2</sub><sup>•-</sup>, through the Fenton reaction but may also be involved in amyloid formation and toxicity in mammals (2–4). Therefore, the total and bioavailable concentrations of Cu inside the cell are thought to be strictly regulated by a Cu homeostasis system, which includes Cu transporters, chaperones, scavengers, and regulatory proteins.

Recent findings suggest that, like iron, copper and copper homeostasis related proteins can be required for full virulence of pathogenic bacteria. For example, a Cu-efflux P-type ATPase CtpA in *Listeria monocytogenes* is a reported virulence factor as is Cu-superoxide dismutase in *Mycobacterium tuberculosis* (*Mtb*) (5, 6). Furthermore, recent microarray studies carried out with *Mtb* at different Cu

concentrations suggest a strong relationship between Cu toxicity and oxidative stress, the latter of which is one of the challenges *Mtb* encounters during its survival in macrophages (7). A proteomics study carried out in *Lactococcus lactis* identified three oxidative stress related proteins as highly induced by Cu stress (8). Although precisely how Cu stress induces an oxidative stress response is not firmly established, the reversible redox cycling of excess Cu in an aerobic environment may well be at least partly causative; in any case, proteins involved in Cu homeostasis have been shown to play important roles in the defense mechanisms of the pathogens against oxidative stress (9, 10).

*Bacillus subtilis* CsoR<sup>1</sup> (*Bsu* CsoR) has recently been found to be a Cu sensor that regulates the transcription of *copZA* operon, which encodes the Cu chaperone CopZ and the Cu-efflux P-type ATPase CopA (11). *Bsu* CsoR shares high sequence similarity with *M. tuberculosis* CsoR (*Mtb* CsoR), the first characterized member of what is predicted to be a large family of Cu regulatory proteins in bacteria (Figure 1) (12). It has been shown that *Bsu* CsoR specifically binds to a pseudopalindromic DNA in the operator–promoter region of *copZA* operon and represses the transcription. Addition of Cu inhibits the binding and derepresses the

<sup>†</sup> This work was supported by grants from the National Institutes of Health to D.P.G. (GM042569) and R.A.S. (GM042025).

\* To whom correspondence should be addressed. E-mail: giedroc@indiana.edu. Tel: 812-856-5449. Fax: 812-856-5710.

<sup>‡</sup> Indiana University.

<sup>§</sup> Texas A&M University.

<sup>||</sup> University of Georgia.

<sup>1</sup> Abbreviations: CsoR, copper-sensitive operon repressor; DTNB, 5,5'-dithiobis(2-nitrobenzoic acid); mag-fura-2, 2-[6-[bis(carboxymethyl)amino]-5-(carboxymethoxy)-2-benzofuranyl]-5-oxazolecarboxylic acid.

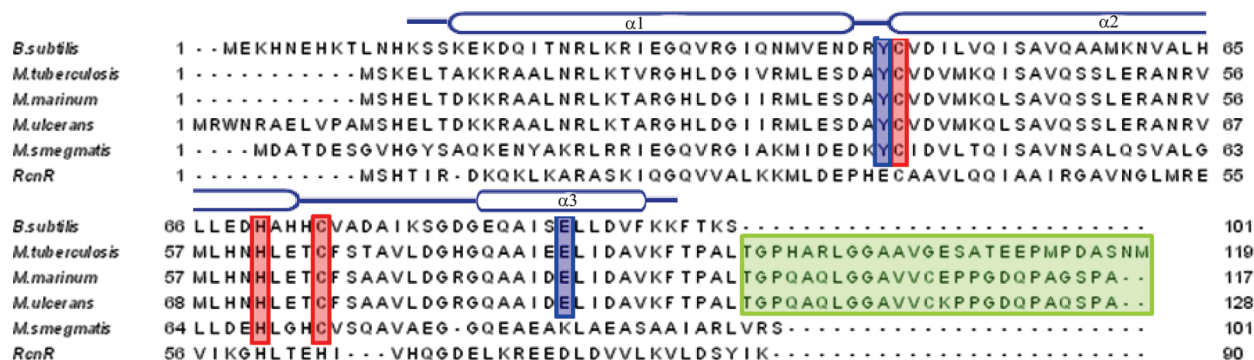


FIGURE 1: Multiple sequence alignment of known CsoR/RcnR family Cu-sensing CsoR homologues from several mycobacteria, *Bsu* CsoR (11) and *E. coli* RcnR (13). Organisms and locus tags (in parentheses) for the other entries are as follows: *M. tuberculosis* (Rv0967) (12); *M. marinum* (MM4874); *M. ulcerans* (MUL\_0425); *M. smegmatis* (MSMEG\_0230). Conserved metal binding residues are highlighted in red, and proposed key residues for allosteric regulation of DNA binding are in blue. The unique C-terminal tails from CsoR homologues encoded by pathogenic mycobacteria are shaded in green. Secondary structure elements are labeled according to *Mtb* CsoR structure (12).

transcription, allowing the expression of CopZ/CopA proteins to traffic and efflux the excess Cu from the cytosol.

The Ni(II)/Co(II) sensor RcnR from *Escherichia coli* is a distant orthologue of *Mtb* CsoR (Figure 1). RcnR regulates the expression of a Ni-efflux system in *E. coli* (13). Recent studies show that RcnR binds Ni(II)/Co(II) with a higher coordination number ( $n = 5$  or  $6$ ) relative to the trigonal planar Cu(I) site ( $n = 3$ ) in *Mtb* CsoR and is proposed to utilize a subset of CsoR Cu ligands as Ni(II)/Co(II) ligands in RcnR (12, 14). This observation, coupled with other CsoR/RcnR orthologues for which we have no biological or structural insight, opens up opportunities to understand the mechanisms of ligand (metal) selectivity at the molecular level, while expanding the range of known functions in this new family of proteins (14).

Here, using a series of biochemical and biophysical experiments, we show that *Bsu* CsoR binds 1 mol equiv of Cu(I) per monomer with very high affinity ( $\geq 10^{21} \text{ M}^{-1}$ ) in vitro. X-ray absorption spectroscopy (XAS) shows Cu(I) adopts, as expected, an  $S_{2N}$  coordination geometry similar to *Mtb* CsoR (12). Both apo and Cu(I)-bound *Bsu* CsoRs are nondissociable tetramers in the low micromolar monomer concentration range. Size exclusion chromatography reveals apo-*Bsu* CsoR binds a 30 bp *copZA* operator DNA with a stoichiometry of 8 monomers, or 2 tetramers, to one 2-fold symmetric, pseudopalindromic DNA sequence. The stepwise DNA binding affinities were further determined by fluorescence anisotropy for both apo-*Bsu* CsoR and Cu(I)-bound *Bsu* CsoR. The Cu(I)-dependent regulation of DNA binding is abrogated in an E90A mutant. Interestingly, *Bsu* CsoR is also capable of binding other divalent metal ions including Co(II), Zn(II), and Ni(II) and, in fact, binds Ni(II) and Zn(II) with  $10^8$ – $10^9 \text{ M}^{-1}$  affinities at equilibrium. However, each of these metals adopts a non-native (nontrigonal) coordination geometry, and each fails to strongly negatively regulate operator DNA binding in vitro.

## METHODS

**Plasmid Construction, Protein Expression, and Purification.** The *Bsu* CsoR-pET16b expression plasmid was a generous gift of Dr. John D. Helmann (Cornell University). Amino acid substitutions were introduced to the plasmid by site-directed quick-change mutagenesis, and the resulting

plasmids were confirmed by DNA sequencing. Wild-type and E90A *Bsu* CsoRs were expressed and purified using similar procedures as described previously for *Mtb* CsoR (11, 12). Expression plasmids containing wild-type or mutant *Bsu* CsoR were transformed into *E. coli* BL21(DE3) and grown in LB media until  $OD_{600}$  reached 0.6–0.8. IPTG (0.4 mM) was then added, and cells were grown for an additional 2 h before harvesting by low-speed centrifugation. Cell pellets were suspended in 200 mL of buffer A (25 mM MES, 2 mM DTT, 1 mM EDTA, pH 5.8) and lysed by sonication. The lysate was centrifuged, and 0.15% (v/v) polyethylenimine (PEI) was added to the supernatant to precipitate the nucleic acids. *Bsu* CsoR remained in the supernatant and was subjected to  $(\text{NH}_4)_2\text{SO}_4$  precipitation, and the ammonium sulfate pellet was resuspended in buffer A and dialyzed against buffer A containing 0.05 M NaCl. The sample was then purified by SP Fast Flow, Superdex 200 size exclusion chromatography as described previously (12). The resultant proteins were pooled, concentrated, and dialyzed against buffer S (10 mM MES, 0.2 M NaCl, pH 6.5) in an anaerobic Vacuum Atmospheres glovebox. The purity of the final products was estimated by visualization of Coomassie-stained 18% Tris–glycine SDS–PAGE gels to be  $\geq 90\%$ . Protein concentration was determined by UV absorption using  $\epsilon_{280\text{nm}} = 1615 \text{ M}^{-1}\text{cm}^{-1}$ , and free thiols were determined by DTNB assay to be more than 95% of the expected value (11, 12). Less than 0.1% copper was detected by atomic absorption spectroscopy in all purified protein samples.

**Cu(I) Binding and BCS Competition Monitored by UV–Vis Absorption Spectroscopy.** Aliquots (250  $\mu\text{L}$ ) of 20  $\mu\text{M}$  *Bsu* CsoR monomer with or without 50  $\mu\text{M}$  bathocuprionedisulfonate (BCS) in buffer S were prepared in an anaerobic glovebox. Different amounts of CuCl were added to each aliquot, and UV–vis absorption spectrum was taken. Samples with BCS were equilibrated in the glovebox at room temperature ( $\approx 22^\circ\text{C}$ ) for 4 h before recording the spectrum to ensure that equilibrium was reached. Absorption at 240 and 483 nm was plotted against Cu concentration, respectively. Cu(I) binding affinity was determined by fitting the BCS competition data by a simple competition model using Dynafit (15) with the overall affinity constant  $K_{\text{Cu(BCS)}_2}$  ( $\beta_2$ ) fixed at  $10^{19.6} \text{ M}^{-2}$ . This value is corrected to pH 6.5 (the pH used here) from the reported value of  $\beta_2 = 19.8$  measured at pH 8.0 ( $\text{p}K_a = 5.7$ ) (16).

**Cu(I) Binding Monitored by Tyrosine Fluorescence.** Ten micromolar *Bsu* CsoR (1700  $\mu$ L) was loaded into an anaerobic cuvette fitted with an adjustable-volume Hamilton gastight syringe loaded with 100  $\mu$ L of Cu(I) titrant prior to removal from the anaerobic glovebox. Emission spectra from 295 to 400 nm were taken at each *i*th addition of Cu(I) with  $\lambda_{\text{ex}} = 280$  nm. The ratio of emission intensity at 307 nm after the *i*th addition (*I*) with the initial intensity (*I*<sub>0</sub>) was plotted against Cu(I) concentration after correcting for dilution (17). No significant photobleaching of the Tyr fluorescence was observed in these experiments.

**Cu(I) X-ray Absorption Spectroscopy.** Both wild-type and E90A *Bsu* CsoRs were mixed with 0.8 mol equiv of Cu(I) in 10 mM MES, 0.2 M NaCl, and 30% (v/v) glycerol, pH 6.5, in an anaerobic environment to about 1 mM final protein concentration. Samples were loaded into a five-well polycarbonate XAS cuvette and immediately frozen in liquid N<sub>2</sub>. XAS data were collected at Stanford Synchrotron Radiation Lightsource (SSRL) on beamline 9-3 with the SPEAR storage ring operating at 3.0 GeV. EXAFS data analysis was performed using EXAFSPAK software, using *ab initio* phase and amplitude functions computed with FEFF v7.2, according to standard procedures as described before (17). Given the minor contribution of Cu–N/O scattering to EXAFS that is dominated by Cu–S, models used for curve fitting contained a fixed Cu–N/O distance that is expected for 3-coordinated Cu(I) imidazole coordination (2.05 Å).

**Sedimentation Velocity and Equilibrium Experiments.** All analytical ultracentrifugation experiments were carried out using a Beckman model Optima XL-I analytical ultracentrifuge equipped with an An-60 Ti rotor in the Physical Biochemistry Instrumentation Facility at Indiana University. All samples were prepared in buffer S and loaded into centerpieces inside the anaerobic glovebox. Samples (110  $\mu$ L) for equilibrium experiments were prepared at 8, 14, and 20  $\mu$ M monomer concentrations (about 0.3, 0.5, and 0.8 OD<sub>230</sub> initially) and loaded into six-channel Epon charcoal-filled centerpieces. Intensity scans at 230 nm were taken at speeds of 19300, 30600, and 38700 rpm at 20 °C. All equilibrium data were fit globally to a single species model using Ultrascan as described (18). For sedimentation velocity experiments, 450  $\mu$ L samples were loaded into a two-channel aluminum centerpiece with 1.2 cm path length. The rotor speed was 60000 rpm at 20 °C, and intensity data at 230 nm were collected as a function of time. Sample concentrations were 8 and 20  $\mu$ M *Bsu* CsoR monomer ( $\approx$ 0.3 and 0.8 OD<sub>230</sub> initially). Data were analyzed using Ultrascan software interfaced with a genetic algorithm and Monte Carlo analysis package essentially as described (19–22).

**Size Exclusion Chromatography.** A 30 bp DNA derived from the *copZA* operator–promoter region (5′-TTGTAATAC-CCTACGGGGGTATGGTAGGAT-3′ and the complementary sequence) was used for all DNA binding experiments. Ten micromolar DNA was mixed with different concentrations of *Bsu* CsoR monomer up to 100  $\mu$ M in buffer S with 2 mM DTT at room temperature. Each mixture (100  $\mu$ L) was loaded onto a Tricon Superdex 200 column (GE healthcare) on an Akta purifier. Elution profiles were obtained by monitoring the absorption at 240, 260, and 280 nm simultaneously.

**Fluorescence Anisotropy.** A 30 bp 5′-fluorescein-labeled DNA with the same sequence as above was used. The

double-stranded DNA was made by mixing the labeled strand with 1.1 mol equiv of the unlabeled complementary strand. The mixture was heated at 95 °C for 10 min and then slowly cooled to room temperature. Formation of double-stranded DNA was further confirmed by native TBE gel electrophoresis. A typical anisotropy experiment was done with 4 nM DNA in 10 mM MES, 0.4 M NaCl, and 2 mM DTT, pH 6.5, at 25 °C unless noted otherwise. Anisotropy was monitored by exciting the fluorescein at 487 nm. With apo or Cu(I)-bound *Bsu* CsoRs added, the average anisotropy of five measurements was reported for each addition. For Ni(II)- and Zn(II)-bound *Bsu* CsoRs, 1 mol equiv of metal ions was mixed with *Bsu* CsoR as titrant; an additional 5  $\mu$ M Ni(II) or Zn(II) was present in the cuvette to ensure that only the metal-bound CsoR was present during these titrations. The resulting data were fitted to a stepwise model involving the binding of two nondissociable tetramers to one DNA using Dynafit, assuming a linear change in anisotropy with fractional saturation of the DNA (15, 17). Since Cu(I)-bound *Bsu* CsoR does not reach saturation, the maximum anisotropy value was fixed at the same value as that obtained for apo-*Bsu* CsoR. The coupling free energy,  $\Delta G_c$ , is operationally defined by  $\Delta G_c = -RT \ln(K_1^{\text{Cu}} K_2^{\text{Cu}} / K_1^{\text{apo}} K_2^{\text{apo}})$ , where  $K_1^{\text{apo}}$ ,  $K_2^{\text{apo}}$ ,  $K_1^{\text{Cu}}$ , and  $K_2^{\text{Cu}}$  are stepwise DNA binding constants for apo and Cu(I)-bound *Bsu* CsoRs, respectively. This formalism for  $\Delta G_c$  was used since the saturating and presumably fully repressing complex invokes two bound tetramers bound per palindromic operator DNA segment, as well as the high inverse correlation between the magnitudes of  $K_1$  and  $K_2$ .

**Other Metal Binding Experiments.** Zn(II) binding was monitored by a chelator competition assay with mag-fura-2 ( $K_{\text{Zn}} = 5.0 \times 10^7 \text{ M}^{-1}$  at pH 7.0) using UV–vis absorption spectroscopy as previously described (17, 18). The data were fit using a competitive binding model with Dynafit (15) to determine the Zn(II) binding affinity. Co(II) and Ni(II) binding experiments were carried out as described previously (17, 18) in buffer S. Ni(II) binding affinity was determined by a competition assay with EGTA (23). All concentrations of metal titrants were determined using atomic absorption spectroscopy.

## RESULTS

***Bsu* CsoR Binds 1 Monomer Mol Equiv of Cu(I) with an Affinity Higher than That of BCS.** It has been previously shown that *Bsu* CsoR regulates the expression of *copZA* operon by binding to the promoter region and that the addition of CuSO<sub>4</sub> and DTT as reductant resulted in disruption of the DNA binding. It was therefore proposed that the DNA binding affinity of *Bsu* CsoR is regulated by Cu(I) binding. Here, we show that *Bsu* CsoR binds Cu(I) directly in vitro by both UV–vis and tyrosine fluorescence spectroscopies.

Addition of Cu(I) into an anaerobic solution of *Bsu* CsoR causes increased absorption in the ultraviolet region ( $\epsilon_{240\text{nm}} \approx 16000 \text{ M}^{-1} \text{ cm}^{-1}$ ); this reports on the formation of thiolate–copper coordination bonds, and the spectrum is quite similar to that of Cu(I)-saturated *Mtb* CsoR (12, 17). This increase is saturable at about 1.0 mol equiv of Cu(I) per monomer (Figure 2A). Significant quenching of tyrosine fluorescence, the importance of which is further discussed



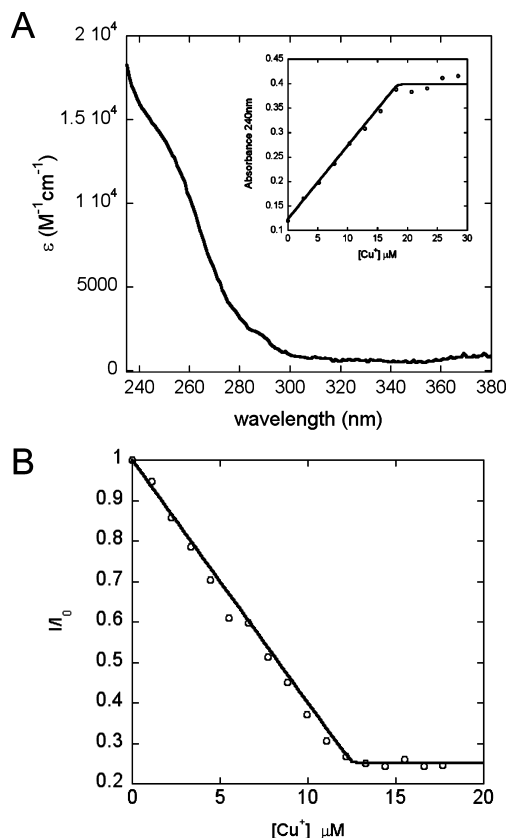


FIGURE 2: *Bsu* CsoR binds 1 mol equiv of Cu(I). (A) Apoprotein-subtracted molar absorptivity spectrum of Cu(I):*Bsu* CsoR mixture at 1:1 molar ratio with the binding isotherm shown in the inset. (B) Anaerobic titration of 10  $\mu M$  apo-*Bsu* CsoR with Cu(I) as monitored by change in tyrosine fluorescence. Conditions: 10 mM MES, 0.2 M NaCl, pH 6.5, 25 °C.

below (see Discussion), is observed upon Cu(I) binding as shown in Figure 2B. Maximum quenching is achieved upon addition of about 1.2 mol equiv of Cu(I). Therefore, both UV-vis and tyrosine fluorescence suggest *Bsu* CsoR binds  $\approx 1$  Cu(I) ion per mole of monomer.

The Cu(I) binding affinity was estimated by a competition experiment using BCS, a Cu(I) specific competitor which can form a  $Cu(I)(BCS)_2$  complex that absorbs at 483 nm with a  $\beta_2 = 19.8$  (16). Figure 3 shows the change of the absorbance at 483 nm when Cu(I) is added to a mixture of 20  $\mu M$  *Bsu* CsoR monomers and 50  $\mu M$  BCS. No change of absorbance is observed until about 20  $\mu M$  Cu(I) is added, suggesting the Cu(I) added initially is bound to *Bsu* CsoR but not BCS. After *Bsu* CsoR is saturated with 1 mol equiv of Cu(I), additional Cu(I) forms a complex with BCS reported by the linear increase of absorbance at 483 nm, which is saturated at about 45  $\mu M$  total Cu(I), reporting on the formation of  $\approx 25 \mu M$   $Cu(I)(BCS)_2$  complex. The fact that no  $Cu(I)(BCS)_2$  complex is formed until saturation of *Bsu* CsoR suggests that *Bsu* CsoR binds Cu(I) with much higher affinity than BCS. Due to the sharpness of the transition, this binding isotherm provides only a lower limit of the apparent binding affinity of  $K_{Cu} \geq 10^{21} M^{-1}$  when fit to a single site binding model [1:1 Cu(I) per protomer] under these solution conditions (see Methods, Table 2). Although CsoR is a tetramer, microscopic binding constants for individual sites in the tetramer, and thus any cooperativity of metal binding to these sites, cannot be resolved by this

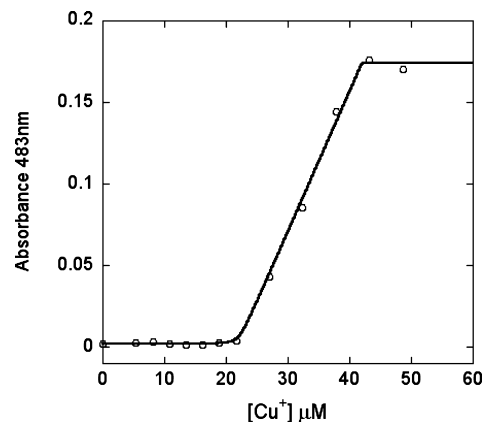


FIGURE 3: BCS competition experiment with wild-type *Bsu* CsoR. Different amounts of Cu(I) were mixed with 20  $\mu M$  *Bsu* CsoR monomer and 50  $\mu M$  BCS in buffer S with the absorbance at 483 nm plotted against the total Cu(I) concentration. The solid curve represents the best fit to a simple competition model (see text for details).

assay under these conditions given the stoichiometric nature of the complex formation.

*Cu(I) Forms a Trigonal  $S_2N$  Coordination Site in Bsu CsoR.* Copper K-edge X-ray absorption spectroscopy was used to determine the structure of Cu(I) complex formed at 0.8:1 Cu(I):*Bsu* CsoR monomer molar ratio (chosen to ensure that all Cu(I) was bound to protein). The preedge peak at 8940 eV in the edge spectrum shown in Figure 4A is consistent with a  $1s \rightarrow 4p$  excitation typical for 3-coordinate Cu(I) (24). The Cu K-edge extended X-ray absorption fine structure (EXAFS) spectrum as well as the Fourier transforms are shown in panels B and C of Figure 4, respectively; structural parameters derived from EXAFS curve fitting are shown in Table 1. The data are best fit to a 3-coordinate model, with two Cu–S interactions at 2.20 Å and a single Cu–N/O interaction (fixed at 2.05 Å). This Cu–S distance is consistent with 3-coordinate Cu(I) and is similar to the Cu–S distance previously reported for *Mtb* CsoR. Significant outer-shell scattering observed between 3 and 4 Å is consistent with the third coordinating ligand being a nitrogen atom from a His residue, possibly from His70 which corresponds to known Cu(I) ligand His61 in *Mtb* CsoR (Figure 1) (12). These data are consistent with the idea that Cu(I) is coordinated by Cys45', His70, and Cys74 in *Bsu* CsoR within a dimer, which are analogous to the Cu(I) ligands in *Mtb* CsoR dimer (Figure 1). Virtually identical spectra and curve-fitting results were obtained for E90A *Bsu* CsoR, suggesting no significant change in the first-shell coordination of Cu(I) in this mutant (see Discussion).

*Both Apo and Cu(I)-Bound Bsu CsoR Are Tetramers.* A preliminary characterization using Superdex 200 size exclusion chromatography on both apo and Cu(I)-bound *Bsu* CsoR revealed a single species roughly corresponding to a homotetramer in both cases (data not shown). To better characterize the assembly state of *Bsu* CsoR in solution, analytical sedimentation equilibrium and velocity ultracentrifugation experiments were carried out with apo and Cu(I)-bound *Bsu* CsoRs in the low micromolar monomer concentration range.

The equilibrium scans were globally fit with a single ideal species model, with representative data and fits shown for the apo and Cu(I)-bound *Bsu* CsoRs in panels A and B of

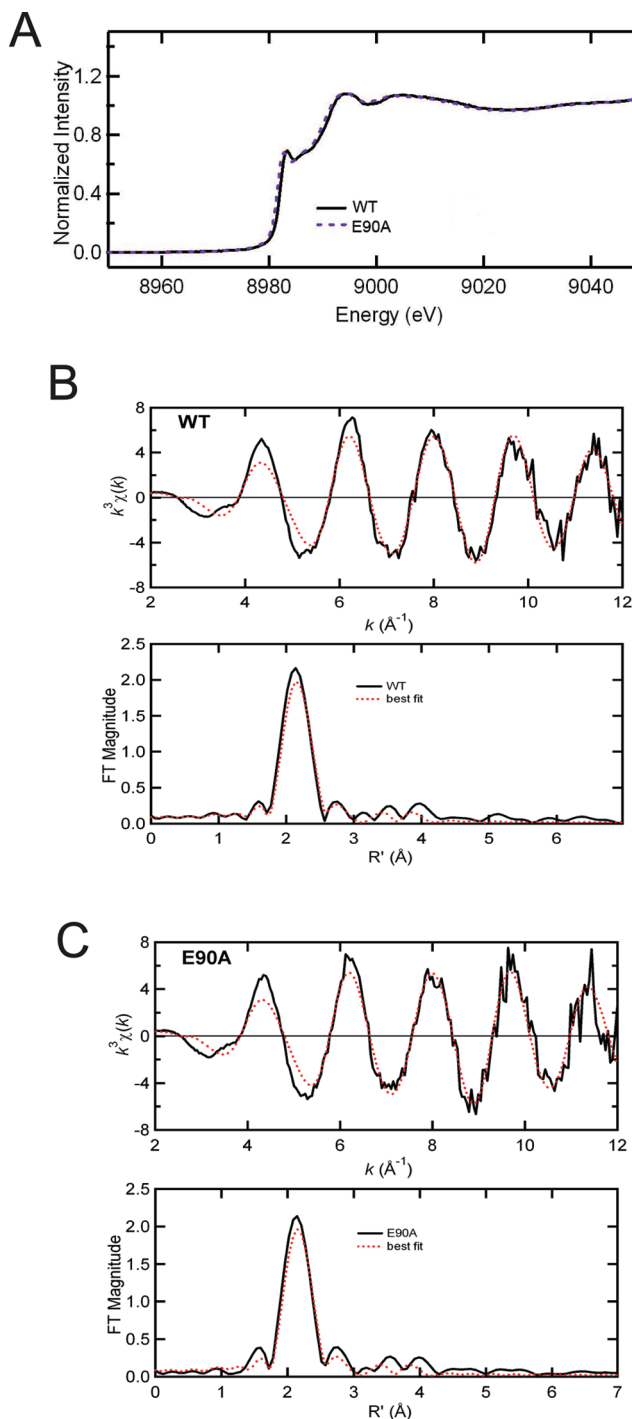


FIGURE 4: X-ray absorption spectroscopy (XAS) of Cu(I)-bound *Bsu* CsoR. (A) Cu K-edge X-ray absorption edge spectra of Cu(I)-bound WT *Bsu* CsoR (solid) and E90A mutant (dashed). Copper K-edge EXAFS spectra and the Fourier transforms ( $k^3$  weighted,  $k = 2-12 \text{ \AA}^{-1}$ ) for Cu(I)-bound WT *Bsu* CsoR (B) and the E90A mutant (C). In panels B and C, solid curves represent the experimental data, and dashed curves represent best fits with parameters compiled in Table 1.

Figure 5, respectively. For apo and Cu(I)-bound *Bsu* CsoR, the single species molecular masses of  $41.0 \pm 0.5$  and  $39.8 \pm 0.6$  kDa, respectively, were obtained. This suggests that the assembly state of both forms of CsoR is tetrameric under these solution conditions (expected molecular mass of 45.9 kDa), and a lower limit of the dimer–tetramer equilibrium constant is  $10^7 (\text{M dimer})^{-1}$ . This is in full agreement with results for the Ni(II)/Co(II) sensor *E. coli* RcnR (14), but

Table 1: XAS Fitting Parameters<sup>a</sup>

sample ( $k$ range)	$\Delta k^3\chi$	fit	shell	$R_{\text{as}}$ (Å)	$\sigma_{\text{as}}^2$ (Å <sup>2</sup> )	$\Delta E_0$ (eV)	$f'^b$
WT <i>Bsu</i> CsoR ( $k = 2-12 \text{ \AA}^{-1}$ ) $\Delta k^3\chi = 12.729$		1	Cu–S <sub>2</sub>	2.20	0.0023	–3.853	0.070
			Cu–N <sub>1</sub>	<u>2.05</u> <sup>c</sup>	<u>0.0016</u>	[–3.853] <sup>d</sup>	
			Cu–C <sub>1</sub>	[3.04]	[0.0032]	[–3.853]	
			Cu–C <sub>1</sub>	[3.08]	[0.0033]	[–3.853]	
			Cu–N <sub>1</sub>	[4.21]	[0.0020]	[–3.853]	
E90A <i>Bsu</i> CsoR ( $k = 2-12 \text{ \AA}^{-1}$ ) $\Delta k^3\chi = 14.157$		1	Cu–S <sub>2</sub>	2.20	0.0024	–4.322	0.076
			Cu–N <sub>1</sub>	<u>2.05</u>	<u>0.0016</u>	[–4.322]	
			Cu–C <sub>1</sub>	[3.04]	[0.0032]	[–4.322]	
			Cu–C <sub>1</sub>	[3.08]	[0.0033]	[–4.322]	
			Cu–N <sub>1</sub>	[4.21]	[0.0020]	[–4.322]	
			Cu–C <sub>1</sub>	[4.24]	[0.0020]	[–4.322]	

<sup>a</sup> Shell is the chemical unit defined for the multiple scattering calculation. Subscripts denote the number of scatterers per metal.  $R_{\text{as}}$  is the metal–scatterer distance.  $\sigma_{\text{as}}^2$  is a mean square deviation in  $R_{\text{as}}$ .  $\Delta E_0$  is the shift in  $E_0$  for the theoretical scattering functions. <sup>b</sup>  $f'$  is a normalized error (chi-squared):  $f' = (\{\sum_i [k^3(\chi_i^{\text{obs}} - \chi_i^{\text{calc}})]^2 / N\}^{1/2}) / [(k^3\chi^{\text{obs}})_{\text{max}} - (k^3\chi^{\text{obs}})_{\text{min}}]$ . <sup>c</sup> Underlined numbers were fixed at the indicated value (not optimized). <sup>d</sup> Numbers in square brackets were constrained to be either a multiple of the above value ( $\sigma_{\text{as}}^2$ ) or to maintain a constant difference from the above value ( $R_{\text{as}}$ ,  $\Delta E_0$ ).

distinct from what we reported for *Mtb* CsoR, where a significant dimer–tetramer equilibrium was observed (12). One possible explanation is that the dimer–tetramer equilibrium of *Mtb* CsoR is influenced by the 30 amino acid C-terminal tail found only in CsoR homologues from pathogenic mycobacteria (see Figure 1).

To confirm the assembly state and obtain further insight into the hydrodynamic properties of the apo and Cu(I)-bound tetramers, sedimentation velocity experiments were carried out under the same solution conditions. Consistent with the equilibrium experiments, a single boundary was observed for all samples; quantitative analysis of these distribution plots is consistent with a single species of sedimentation coefficient 3.03 S for apo-*Bsu* CsoR and 3.34 S for Cu(I)-bound *Bsu* CsoR (panels C and D of Figure 5, respectively). The fitted parameters and predicted hydrodynamic characteristics are compiled in Table 3. These data taken collectively suggest that the dominant assembly state of each form of CsoR is that of a highly asymmetric tetramer with Cu(I) binding inducing a small but measurable change in the hydrodynamic properties of the molecule (see Discussion).

**Apo-*Bsu* CsoR Binds Operator DNA with 2:1 Tetramer: DNA Stoichiometry.** It was previously shown that *Bsu* CsoR is capable of binding to an operator in the promoter of *copZA* operon, although the stoichiometry and affinity were not investigated in detail (11). Size exclusion chromatography was first used to determine the DNA binding stoichiometry (Figure 6A). Addition of 40  $\mu\text{M}$  apo-*Bsu* CsoR monomer to 10  $\mu\text{M}$  DNA gives rise to a new peak with an elution volume of 13.7 mL, assigned to a *Bsu* CsoR–DNA complex, with a significant fraction of DNA. Addition of 80  $\mu\text{M}$  apo-*Bsu* CsoR monomer to 10  $\mu\text{M}$  DNA reveals that only the 13.7 mL peak is observed with no evidence of free DNA, suggesting that all the protein and DNA added form the complex. Further addition of protein does not affect the protein–DNA complex peak at 13.7 mL, with only free protein peak eluting at 15.9 mL (data not shown). This suggests that the *Bsu* CsoR–DNA interaction saturates at 8:1 monomer:DNA ratio corresponding to two tetramers per DNA. Similar experiments carried out with Cu(I)-bound *Bsu*

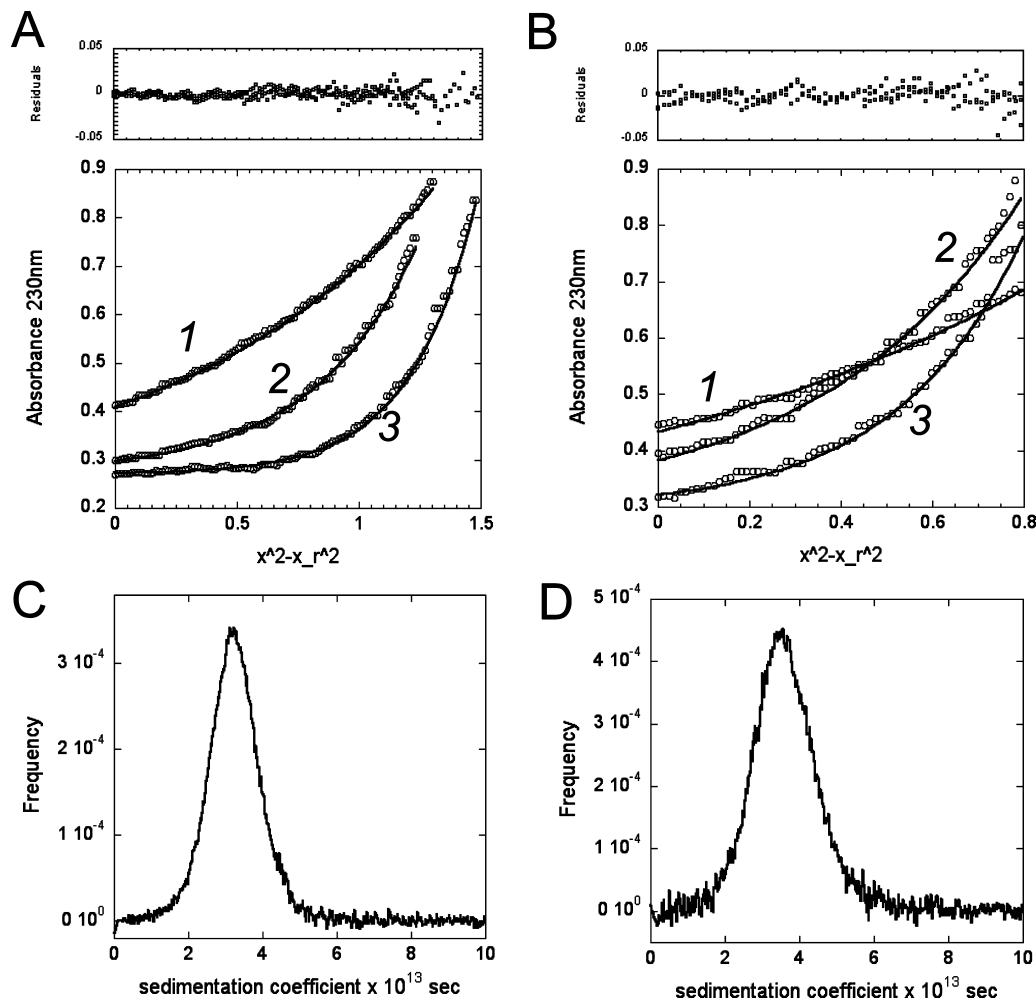


FIGURE 5: Analytical ultracentrifugation of apo and Cu(I)-bound *Bsu* CsoRs. (A, B) Representative equilibrium data with a global fit to a single ideal species model and residuals for both apo and Cu(I)-bound *Bsu* CsoR at 0.3 AU<sub>230</sub>, respectively. The three data sets correspond to different rotor speeds: (1) 19300 rpm; (2) 30600 rpm; (3) 38700 rpm. The solid curves show a global fit to a single ideal species model (residues in upper panel). (C, D) Distribution of sedimentation coefficient of apo and Cu(I)-bound *Bsu* CsoR, respectively. All parameters derived from sedimentation velocity fits are compiled in Table 3.

CsoR reveals the elution of only free DNA and free protein and no protein–DNA complex peak (data not shown), which is consistent with the fact that Cu(I) binding to *Bsu* CsoR significantly decreases its DNA binding affinity.

Fluorescence anisotropy experiments carried out in buffer S (0.2 M NaCl) with 2 mM DTT with 10 nM 30 bp DNA further confirm the stoichiometry. Under these conditions, apo-*Bsu* CsoR binds the fluorescein-labeled 30 bp DNA with very high affinity ( $\geq 10^9$  M<sup>-1</sup>) as revealed by the stoichiometric binding curve (Figure 6B). The binding isotherm increases linearly and saturates at about 8 *Bsu* CsoR monomers to 1 DNA, consistent with the stoichiometry determined by size exclusion chromatography. Since free *Bsu* CsoR is a stable tetramer, these data are consistent with a stoichiometry of two tetramers binding to one 2-fold symmetric DNA.

**DNA Binding Affinity of Apo and Cu(I)-Bound *Bsu* CsoR.** The apparent DNA binding affinity of apo-*Bsu* CsoR was estimated to be  $2 \times 10^7$  M<sup>-1</sup> by electrophoretic mobility shift assay (EMSA) in 20 mM Tris, 50 mM NaCl, and 1 mM DTT at pH 8.0 (11). To determine the binding affinity quantitatively, we performed the fluorescence anisotropy experiments at 0.4 M NaCl in buffer S. Figure 7A shows a typical normalized *Bsu* CsoR–DNA binding curve monitored

by fluorescence anisotropy. Since only a lower limit of tetramerization constant of  $10^7$  M<sup>-1</sup> was determined by analytical ultracentrifugation, these DNA binding data were fit using a stepwise binding model of two nondissociable tetramers to one DNA. Apo-*Bsu* CsoR binds to the DNA with  $K_1^{\text{apo}} = 3.1 (\pm 0.8) \times 10^7$  M<sup>-1</sup> and  $K_2^{\text{apo}} = 8.3 (\pm 2.2) \times 10^7$  M<sup>-1</sup>, while Cu(I)-bound *Bsu* CsoR binds the same DNA with  $K_1^{\text{Cu}} = 2.9 (\pm 0.4) \times 10^6$  M<sup>-1</sup> and  $K_2^{\text{Cu}} \leq 1.0 \times 10^5$  M<sup>-1</sup>. This gives an operationally defined coupling free energy ( $\Delta G_c$ )  $\geq 5.4$  kcal/mol (Table 2). The second binding event was not observed for Cu(I)-bound protein under the experimental conditions; therefore, only an upper limit for  $K_2^{\text{Cu}}$  is reported here.

**DNA Binding by E90A CsoR Is Not Regulated by Cu(I) Binding.** How Cu(I) binding changes the conformation and/or assembly state of CsoR in a way that results in an allosterically inhibited conformation remains unclear; however, previous preliminary observations suggested that a highly conserved residue in the  $\alpha 3$  helix, Glu81 in *Mtb* CsoR, may be crucial in driving this switch (Figure 1) (12). Therefore, to test whether *Bsu* CsoR shares an allosteric mechanism that is similar to that suggested for *Mtb* CsoR, the equivalent residue in *Bsu* CsoR, Glu90, was substituted with an Ala. As shown in Figure 7B, Cu(I)-bound E90A binds the 30 bp DNA with a high affinity

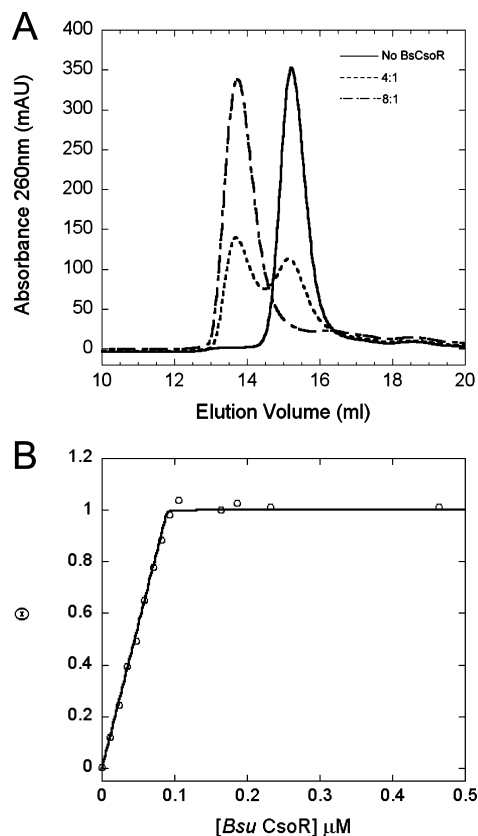


FIGURE 6: *Bsu* CsoR–*copZA* operator DNA binding stoichiometry. (A) Elution profile obtained with different *Bsu* CsoR:DNA ratios from a Superdex 200 column as monitored by absorption at 260 nm. Conditions: 10 mM MES, 0.2 M NaCl, 2 mM DTT, pH 6.5. (B) Normalized fluorescence anisotropy-based DNA binding isotherm (*Bsu* CsoR expressed in monomer concentration) with 10 nM DNA in 10 mM MES, pH 6.5, 0.2 M NaCl, 2 mM DTT, 25 °C.

that is similar in magnitude to that of apo-E90A CsoR, suggesting that Cu(I) binding does not negatively regulate the DNA binding affinity of this mutant. Since the Cu(I) binding affinity (data not shown) and coordination environment of E90A CsoR (Figure 4) are indistinguishable from that of wild-type CsoR, these data suggest that E90 plays an important role in mediating Cu(I)-dependent negative regulation of DNA binding.

**Binding of Zn(II), Co(II), and Ni(II) to *Bsu* CsoR.** Although studies in *Mtb* and in *M. smegmatis* reveal that Cu(I) is the primary inducer of *csoR*-dependent gene expression, it was of interest to determine the specificity of Cu(I) binding and the degree to which other metals could allosterically regulate *copZA* operator–promoter binding. A Zn(II) titration using mag-fura-2 as a competition chelator shows that *Bsu* CsoR binds Zn(II) with  $K_{Zn} = 1.6 (\pm 0.1) \times 10^8 \text{ M}^{-1}$  (see Supporting Information Figure S1A, Table 2). To provide insight into the coordination geometry of Zn(II), Co(II) was used as a structural surrogate for Zn(II) (17, 18). Not surprisingly, Co(II) binds to *Bsu* CsoR with an affinity far lower than that of Zn(II), with  $K_{Co} \leq 10^5 \text{ M}^{-1}$  under the same conditions. As shown in Figure 8A, Co(II)-bound *Bsu* CsoR shows strong ligand-to-metal charge transfer (LMCT) at 290 nm with an  $\epsilon = 1500 \text{ M}^{-1} \text{ cm}^{-1}$  and at 335 nm with an  $\epsilon = 800 \text{ M}^{-1} \text{ cm}^{-1}$ . The d–d transition envelope centered at  $\approx 600 \text{ nm}$  gives an  $\epsilon \approx 300 \text{ M}^{-1} \text{ cm}^{-1}$ . These data taken together are consistent with a tetrahedral or distorted tetrahedral Co(II) complex with one or two of the Cys

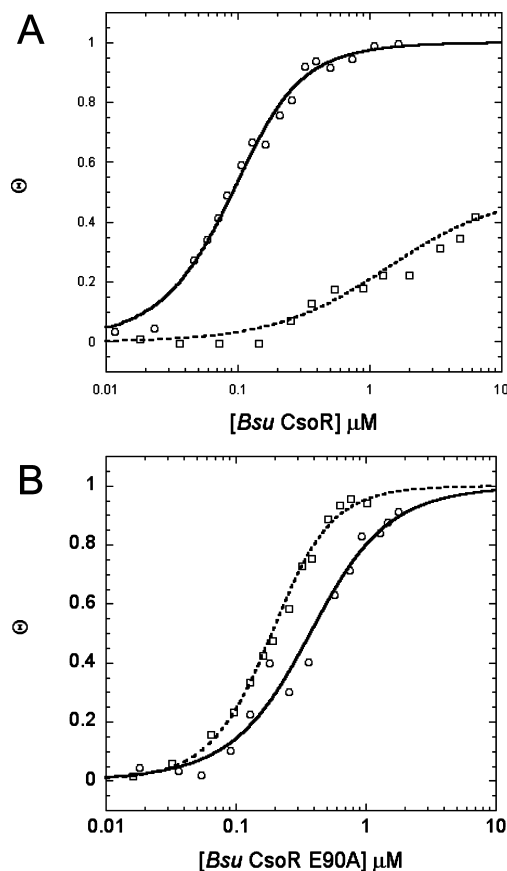


FIGURE 7: Normalized fluorescence anisotropy-based DNA binding isotherms of WT (A) and E90A (B) *Bsu* CsoRs (expressed as CsoR monomer concentration) acquired in the absence (O) and presence (□) of Cu(I). Curves represent the best fit using a stepwise two tetramer DNA binding model with the fitting parameters given in Table 2.

residues as donor atoms to the Co(II). Since Co(II) is bound tetrahedrally, Zn(II) may well bind with the same coordination geometry, although this was not directly determined here.

When apo-*Bsu* CsoR binds Ni(II), the UV–vis absorption spectrum shows a feature at  $\approx 480 \text{ nm}$  with a molar intensity of  $\epsilon = 100 \text{ M}^{-1} \text{ cm}^{-1}$  (Figure 8B and inset). This feature is consistent with a square planar or distorted square planar coordination geometry as observed previously for *E. coli* NikR (23) and nickel-substituted mutant retroviral-type zinc-finger peptides (25). The intense charge transfer transitions in the near-ultraviolet region suggest that Cys residues are involved in coordinating Ni(II). The binding isotherm as shown in the inset of Figure 8B shows a linear increase up to about 1.2 mol equiv of Ni(II) followed by a sharp transition to a plateau, revealing that *Bsu* CsoR binds  $\approx 1$  mol equiv of Ni(II) with a binding affinity  $\geq 10^7 \text{ M}^{-1}$  (i.e., stoichiometrically). The binding affinity estimated by an EGTA competition experiment was determined to be  $K_{Ni} = 3.6 (\pm 0.3) \times 10^9 \text{ M}^{-1}$  (see Table 2, Supporting Information Figure S1B).

These metal binding experiments clearly show that *Bsu* CsoR is also capable of binding other divalent metal ions with widely different affinities and coordination geometries. To test whether these metal ions are significant allosteric negative effectors of DNA binding, fluorescence anisotropy experiments analogous to that shown in Figure 7 for Cu(I) were carried out with excess metal ion to ensure that the



Table 2: Summary of Metal and DNA Binding Affinities and Allosteric Coupling Free Energies for Metallo Derivatives of Wild-Type and E90A *Bsu* CsoR

<i>Bsu</i> CsoR	metal	metal binding affinity <sup>a</sup> (M <sup>-1</sup> )	DNA binding affinity <sup>b</sup>		$\Delta G_c$ (kcal/mol)
			$K_1$ (M <sup>-1</sup> )	$K_2$ (M <sup>-1</sup> )	
wild type	apo		$3.1 (\pm 0.8) \times 10^7$	$8.3 (\pm 2.2) \times 10^7$	
	Cu(I)	$\geq 10^{21}$	$2.9 (\pm 0.4) \times 10^6$	$\leq 1.0 \times 10^5$	$\geq +5.4$
	Co(II)	$\leq 10^5$			
	Ni(II)	$3.6 (\pm 0.3) \times 10^9$	$5.7 (\pm 1.0) \times 10^6$	$3.1 (\pm 0.5) \times 10^7$	$+1.6 (\pm 0.3)$
E90A	Zn(II)	$1.6 (\pm 0.1) \times 10^8$ <sup>c</sup>	$1.0 (\pm 0.3) \times 10^7$	$1.5 (\pm 0.4) \times 10^7$	$+1.7 (\pm 0.3)$
	apo		$9.5 (\pm 3.0) \times 10^6$	$1.3 (\pm 0.4) \times 10^7$	
	Cu(I)	$\geq 10^{21}$	$4.8 (\pm 2.0) \times 10^6$	$1.1 (\pm 0.4) \times 10^8$	$-0.9 (\pm 0.4)$

<sup>a</sup> The results of fitting to a simple 1:1 (metal:monomer) binding model. <sup>b</sup> Solution conditions: 10 mM MES, 0.4 M NaCl, 2 mM DTT, pH 6.5, 25 °C. We note that unique values of  $K_1$  and  $K_2$  are not readily resolved in this assay (see Methods). <sup>c</sup> A fit to two-site stepwise dimer binding models gives  $K_{Zn1} = 1.7 (\pm 0.4) \times 10^9$  M<sup>-1</sup>;  $K_{Zn2} = 4.5 (\pm 0.3) \times 10^7$  M<sup>-1</sup> (see Supporting Information Figure S1).

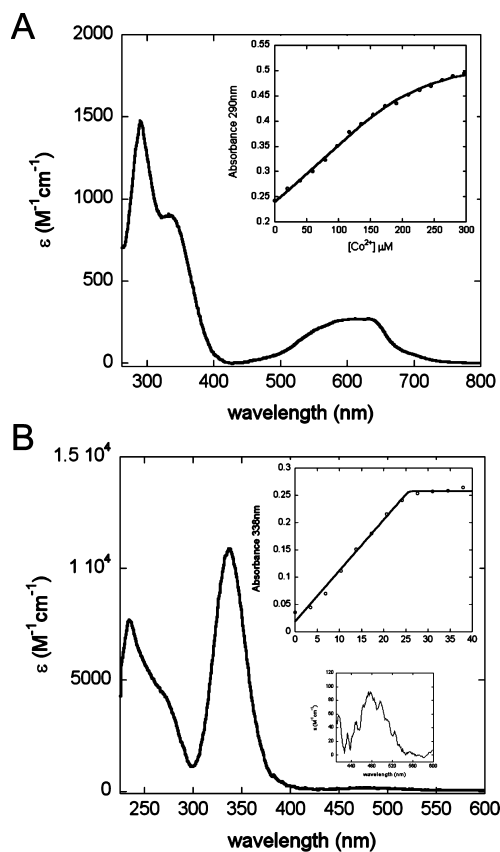


FIGURE 8: Co(II) and Ni(II) binding to *Bsu* CsoR. Apoprotein-subtracted molar absorptivity spectra of Co(II):*Bsu* CsoR mixture at 2:1 molar ratio (A) or Ni(II):*Bsu* CsoR mixture at 1:1 molar ratio (B). The binding isotherms shown in the insets are fitted with a simple 1:1 binding model with parameters collected in Table 2.

metal-bound form of the protein is the predominant species in solution. The fitted parameters are compiled in Table 2. Both Zn(II)- and Ni(II)-complexed *Bsu* CsoR bind to the 30 bp *copZA* operator DNA with affinity close to that of apo-*Bsu* CsoR, each resulting in only a small positive coupling free energy (Supporting Information Figure S2). This is consistent with previous observations that divalent metal ions are poor regulators of DNA binding of *Mtb* CsoR both in vitro and in vivo, despite their high equilibrium affinities for these metals (12).

## DISCUSSION

*Bsu* CsoR regulates the transcription of *copZA* operon, which encodes two important components of the Cu homeo-

stasis system, the Cu-chaperone CopZ and the Cu-effluxer CopA. It is widely accepted that in both eukaryotes and prokaryotes the intracellular trafficking of copper ions is dependent on metallochaperones which reinforces the idea that there is little or no “free” or bioavailable copper ions in the cell (26–28). It is still unclear how *Bsu* CsoR, as a Cu sensor, obtains its copper ion in the cell, although one strong possibility is from CopZ. Such a CopZ-dependent transfer of Cu to *Bsu* CsoR is analogous to the well-studied mechanism in *Enterococcus hirae*, where the Cu-sensor CopY acquires Cu from the Cu-chaperone CopZ (29). Under uninduced conditions, a background level of CopZ in the cell functions as a copper chelator or buffer, perhaps delivering copper to target proteins. The ratio between apo and Cu-bound CopZ may be thermodynamically and kinetically maintained in a certain window by various cellular protein–protein interactions and Cu-transfer reactions. Upon Cu stress, Cu-bound CopZ may be quickly formed, therefore making it possible to transfer Cu to *Bsu* CsoR, leading to derepression of the *copZA* operon; this, in turn, results in increased expression of apo-CopZ and CopA required to efflux excess Cu out of cytosol, bringing this ratio back into a normal or unstressed range. Cu(I)-bound *Bsu* CsoR may then be degraded or potentially transfer Cu to other target proteins, e.g., CopA itself, via a ligand exchange reaction (30).

*Bsu* CsoR and *Mtb* CsoR share very high amino acid sequence identity. In particular, all three proposed Cu ligands are conserved as are two proposed “second shell” residues, corresponding to Tyr35 (Tyr44 in *Bsu*) and Glu81 (Glu90 in *Bsu*) in *Mtb* CsoR. The major difference between the two CsoRs is that *Mtb* CsoR contains a unique  $\approx 30$  amino acid C-terminal tail which is missing in the previously solved crystal structure of Cu(I) CsoR from *Mtb* (Figure 1) (12). Aside from this, these two CsoRs possess very similar biochemical and biophysical properties. Both coordinate 1 monomer mol equiv of Cu(I) with very high affinity to form a trigonal planar  $S_2N$  coordination geometry with very similar Cu–S distances. It is also the case that *Bsu* CsoR is a stable tetramer in the low micromolar (monomer) concentration range, while a dimer–tetramer equilibrium was observed in previous analytical ultracentrifugation studies carried out on full-length *Mtb* CsoR (12). Adjacent  $C_2$ -symmetric dimers in the crystal structure of Cu(I)-bound *Mtb* CsoR pack against one another to form a tetramer with  $D_2$  rotational symmetry. In this configuration of the tetramer, the C-terminal tail of *Mtb* CsoR would be positioned at the dimer–dimer interface; it therefore seems possible that the flexible C-terminal tail



Table 3: Summary of Fitted Parameters Derived from Sedimentation Velocity Experiments with *Bsu* CsoR

CsoR	$s \times 10^{13}$ (s)	$D \times 10^7$ (cm <sup>2</sup> /s)	rmsd	$ff_{f_0}$ <sup>a</sup>
apo (0.3 OD <sub>230</sub> )	3.05	6.84	0.0067	1.50
apo (0.8 OD <sub>230</sub> )	3.01	7.08	0.011	1.52
Cu(I) bound (0.3 OD <sub>230</sub> )	3.34	6.07	0.0082	1.37
Cu(I) bound (0.8 OD <sub>230</sub> )	3.34	6.10	0.0095	1.37

<sup>a</sup> Frictional coefficients calculated from  $s$  and  $D$  upon fixing the molecular mass of the tetramer to 45.9 kDa.

may destabilize the *Mtb* CsoR tetramer toward dimer. This has yet to be investigated systematically.

We find no significant differences in assembly states of the apo and Cu(I)-bound forms of *Bsu* CsoR, which are both tetrameric under the conditions investigated. Therefore, only a lower limit of the tetramerization constant ( $K_{\text{tet}}$ ) of about  $10^7$  (M dimer)<sup>-1</sup> could be estimated from these data. However, differences in  $K_{\text{tet}}$  in the nanomolar concentration range cannot be ruled out by these data; if this is the case, they may be partly responsible for the different DNA binding affinities reported here for apo and Cu(I) CsoR. On the other hand, the sedimentation velocity experiments show a small increase in sedimentation coefficient in Cu(I)-bound *Bsu* CsoR, suggesting a conformation with a smaller frictional coefficient, thus more spherical relative to the apoprotein (Table 3). However, this change may not play a primary role in allosteric regulation of DNA binding because a similar change in sedimentation coefficient appears to characterize the E90A mutant as well (data not shown).

Understanding what happens when a particular metal sensor binds the “wrong” metal is just as important as understanding how the cognate metal ion drives regulation of gene expression (31). We show here that the metal binding site of *Bsu* CsoR can adopt a range of distinct coordination numbers and geometries upon binding different metal ions. Co(II), and by inference Zn(II), adopts a tetrahedral or distorted tetrahedral geometry while Ni(II) appears to form a square planar or distorted square planar geometry. Each complex incorporates one or both Cys residues in *Bsu* CsoR; in fact, it is formally possible that each employs all three Cu(I) ligands while adding a fourth ligand, perhaps from the N-terminal region as in RcnR (14) or from solvent. In any case, the Co(II) and Ni(II) coordination geometries are clearly distinct from that of RcnR, where each metal adopts an octahedral or pseudooctahedral complex (14). Strikingly, while the binding of Cu(I) stabilizes an allosterically inhibited conformation of *Bsu* CsoR, neither Zn(II) nor Ni(II) is capable of strongly regulating the DNA binding, despite their high equilibrium affinities (albeit  $\geq 10$  orders of magnitude smaller than  $K_{\text{Cu}}$ ) (Table 2). In fact,  $K_{\text{Ni}}$  for CsoR may well be comparable to  $K_{\text{Ni}}$  for the *bona fide* Ni/Co sensor *E. coli* RcnR; in contrast,  $K_{\text{Co}}$  is at least  $10^4$  smaller for *Bsu* CsoR ( $K_{\text{Zn}}$  has not been reported for RcnR) (14). These features are consistent with the emerging theme that formation of the “native” coordination geometry is most closely linked to biological metalloregulation, rather than absolute metal binding affinity (18, 32, 33). This, in turn, suggests that specific features of the trigonal planar Cu(I) coordination complex in CsoR may organize a “second coordination shell” of interactions used to drive defined conformational changes that are linked to Cu(I)-mediated derepression of gene expression (12, 17).

One strong candidate for propagating this structural change in Cu(I) CsoRs is the N<sup>ε</sup> face of His70 (His61 in *Mtb* CsoR). The crystal structure of *Mtb* CsoR reveals that this face of the His61 imidazole ring is in close proximity to the side chains of both Glu81 and Tyr35' in *Mtb* CsoR (12), which correspond to Glu90 and Tyr44' in *Bsu* CsoR. Glu90 is a highly conserved residue in the  $\alpha 3$  helix of all Cu(I)-specific CsoRs (Figure 1), and we show here that an Ala substitution abolishes negative regulation of DNA binding without significantly interfering with the Cu(I) affinity or coordination geometry. We note that the significant quenching of the steady-state tyrosine fluorescence upon Cu(I) binding is consistent with a tyrosinate-like species, that might form as a result of hydrogen bonding of its hydroxyl proton with an as yet unidentified acceptor, an excellent candidate for which is Glu90 (34). Interestingly, both of these conserved residues have also been shown to be crucial for allosteric regulation in *Mtb* CsoR (Z. Ma and D. P. Giedroc, unpublished observations).

One model for negative allosteric regulation of DNA binding of CsoR by Cu(I) posits that the  $\alpha 3$  helix is only loosely associated with the  $\alpha 2'$  helix of the four-helical dimer bundle ( $\alpha 1$ - $\alpha 2$ - $\alpha 1'$ - $\alpha 2'$ ) within the dimer and/or tetramer in the absence of Cu(I). This helix may in fact physically interact with the adjacent tetramer when bound to the DNA, thereby stabilizing an octameric assembly state on the DNA. Cu(I) binding to this species may reorient and strongly stabilize the intramolecular  $\alpha 3$ - $\alpha 2'$  interface within a tetramer, leading to a conformation that is not optimized for high-affinity DNA binding and/or forms a limiting 1:1 tetramer:DNA complex that is nonfunctional for repression (see Figure 7). Uninducing metal ions, e.g., Ni(II) and Zn(II), while detectably regulatory (see Table 2) do not block formation of the repressing 2:1 tetramer:DNA complex and are therefore nonfunctional; this model is consistent with the DNA binding characteristics of each metalloderivative of *Bsu* CsoR reported here. Further biochemical and structural support for this proposed mechanism of regulation is required.

## ACKNOWLEDGMENT

We thank Dr. John Helmann, Cornell University, for the gift of the overexpression plasmid for *Bsu* CsoR and Dr. Todd Stone, Indiana University, for help in analyzing the analytical ultracentrifugation experiments. Portions of this research were carried out at the Stanford Synchrotron Radiation Lightsource, a national user facility operated by Stanford University on behalf of the U.S. Department of Energy, Office of Basic Energy Sciences. The SSRL Structural Molecular Biology Program is supported by the Department of Energy, Office of Biological and Environmental Research, and by the National Institutes of Health, National Center for Research Resources, Biomedical Technology Program.

## SUPPORTING INFORMATION AVAILABLE

Competition experiments for Zn(II) and Ni(II) binding to *Bsu* CsoR (Figure S1) and DNA binding curves for Zn(II)- and Ni(II)-bound *Bsu* CsoR (Figure S2). This material is available free of charge via the Internet at <http://pubs.acs.org>.

## REFERENCES

- Davis, A. V., and O'Halloran, T. V. (2008) A place for thioether chemistry in cellular copper ion recognition and trafficking. *Nat. Chem. Biol.* **4**, 148–151.
- Soliz, M., and Stoyanov, J. V. (2003) Copper homeostasis in *Enterococcus hirae*. *FEMS Microbiol. Rev.* **27**, 183–195.
- Dong, J., Atwood, C. S., Anderson, V. E., Siedlak, S. L., Smith, M. A., Perry, G., and Carey, P. R. (2003) Metal binding and oxidation of amyloid-beta within isolated senile plaque cores: Raman microscopic evidence. *Biochemistry* **42**, 2768–2773.
- Meloni, G., Sonois, V., Delaine, T., Guilloreau, L., Gillet, A., Teissie, J., Faller, P., and Vasak, M. (2008) Metal swap between Zn7-metallothionein-3 and amyloid-[beta]-Cu protects against amyloid-[beta] toxicity. *Nat. Chem. Biol.* **4**, 366–372.
- Francis, M. S., and Thomas, C. J. (1997) Mutants in the CtpA copper transporting P-type ATPase reduce virulence of *Listeria monocytogenes*. *Microb. Pathog.* **22**, 67–78.
- Spagnolo, L., Toro, I., D'Orazio, M., O'Neill, P., Pedersen, J. Z., Carugo, O., Rotilio, G., Battistoni, A., and Djinoic-Carugo, K. (2004) Unique features of the sodC-encoded superoxide dismutase from *Mycobacterium tuberculosis*, a fully functional copper-containing enzyme lacking zinc in the active site. *J. Biol. Chem.* **279**, 33447–33455.
- Ward, S. K., Hoyer, E. A., and Talaat, A. M. (2008) The global responses of *Mycobacterium tuberculosis* to physiological levels of copper. *J. Bacteriol.* **190**, 2939–2946.
- Magnani, D., Barre, O., Gerber, S. D., and Soliz, M. (2008) Characterization of the CopR regulon of *Lactococcus lactis* IL1403. *J. Bacteriol.* **190**, 536–545.
- Robinson, N. J. (2008) A bacterial copper metallothionein. *Nat. Chem. Biol.* **4**, 582–583.
- Gold, B., Deng, H., Bryk, R., Vargas, D., Eliezer, D., Roberts, J., Jiang, X., and Nathan, C. (2008) Identification of a copper-binding metallothionein in pathogenic mycobacteria. *Nat. Chem. Biol.* **4**, 609–616.
- Smaldone, G. T., and Helmann, J. D. (2007) CsoR regulates the copper efflux operon copZA in *Bacillus subtilis*. *Microbiology* **153**, 4123–4128.
- Liu, T., Ramesh, A., Ma, Z., Ward, S. K., Zhang, L., George, G. N., Talaat, A. M., Sacchettini, J. C., and Giedroc, D. P. (2007) CsoR is a novel *Mycobacterium tuberculosis* copper-sensing transcriptional regulator. *Nat. Chem. Biol.* **3**, 60–68.
- Iwig, J. S., Rowe, J. L., and Chivers, P. T. (2006) Nickel homeostasis in *Escherichia coli*—the rcnR-rcnA efflux pathway and its linkage to NikR function. *Mol. Microbiol.* **62**, 252–262.
- Iwig, J. S., Leitch, S., Herbst, R. W., Maroney, M. J., and Chivers, P. T. (2008) Ni(II) and Co(II) sensing by *Escherichia coli* RcnR. *J. Am. Chem. Soc.* **130**, 7592–7606.
- Kuzmic, P. (1996) Program DYNAFIT for the analysis of enzyme kinetic data: application to HIV proteinase. *Anal. Biochem.* **237**, 260–273.
- Xiao, Z., Loughlin, F., George, G. N., Howlett, G. J., and Wedd, A. G. (2004) C-terminal domain of the membrane copper transporter Ctr1 from *Saccharomyces cerevisiae* binds four Cu(I) ions as a cuprous-thiolate polynuclear cluster: sub-femtomolar Cu(I) affinity of three proteins involved in copper trafficking. *J. Am. Chem. Soc.* **126**, 3081–3090.
- Liu, T., Chen, X., Ma, Z., Shokes, J., Hemmingsen, L., Scott, R. A., and Giedroc, D. P. (2008) A CuI-sensing ArsR family metal sensor protein with a relaxed metal selectivity profile. *Biochemistry* **47**, 10564–10575.
- Pennella, M. A., Shokes, J. E., Cosper, N. J., Scott, R. A., and Giedroc, D. P. (2003) Structural elements of metal selectivity in metal sensor proteins. *Proc. Natl. Acad. Sci. U.S.A.* **100**, 3713–3718.
- Brookes, E., and Demeler, B. (2008) Parallel computational techniques for the analysis of sedimentation velocity experiments in UltraScan. *Colloid Polym. Sci.* **286**, 139–148.
- Demeler, B., and Brookes, E. (2008) Monte Carlo analysis of sedimentation experiments. *Colloid Polym. Sci.* **286**, 129–137.
- Brookes, E., and Demeler, B. (2006) Genetic algorithm optimization for obtaining accurate molecular weight distributions from sedimentation velocity experiments, in *Analytical Ultracentrifugation*, Vol. VIII, pp 33–40.
- Tan, X., Kagiampakis, I., Surovtsev, I. V., Demeler, B., and Lindahl, P. A. (2007) Nickel-dependent oligomerization of the alpha subunit of acetyl-coenzyme A synthase/carbon monoxide dehydrogenase. *Biochemistry* **46**, 11606–11613.
- Wang, S. C., Dias, A. V., Bloom, S. L., and Zamble, D. B. (2004) Selectivity of metal binding and metal-induced stability of *Escherichia coli* NikR. *Biochemistry* **43**, 10018–10028.
- Kau, L. S., Spira-Solomon, D. J., Penner-Hahn, J. E., Hodgson, K. O., and Solomon, E. I. (1987) X-ray absorption-edge determination of the oxidation-state and coordination-number of copper—application to the type-3 site in rhus-vernificera laccase and its reaction with oxygen. *J. Am. Chem. Soc.* **109**, 6433–6442.
- Chen, X., Chu, M., and Giedroc, D. P. (2000) Spectroscopic characterization of Co(II)-, Ni(II)-, and Cd(II)-substituted wild-type and non-native retroviral-type zinc finger peptides. *J. Biol. Inorg. Chem.* **5**, 93–101.
- Rae, T. D., Schmidt, P. J., Pufahl, R. A., Culotta, V. C., and O'Halloran, T. V. (1999) Undetectable intracellular free copper: the requirement of a copper chaperone for superoxide dismutase. *Science* **284**, 805–808.
- Rosenzweig, A. C., and O'Halloran, T. V. (2000) Structure and chemistry of the copper chaperone proteins. *Curr. Opin. Chem. Biol.* **4**, 140–147.
- Pennella, M. A. C. (2001) Copper delivery by metallochaperone proteins. *Acc. Chem. Res.* **34**, 119–128.
- Cobine, P. A., George, G. N., Jones, C. E., Wickramasinghe, W. A., Soliz, M., and Dameron, C. T. (2002) Copper transfer from the Cu(I) chaperone, CopZ, to the repressor, Zn(II)CopY: metal coordination environments and protein interactions. *Biochemistry* **41**, 5822–5829.
- Banci, L., Bertini, I., Cantini, F., Felli, I. C., Gonnelli, L., Hadjiladis, N., Pierattelli, R., Rosato, A., and Voulgaris, P. (2006) The Atx1-Ccc2 complex is a metal-mediated protein-protein interaction. *Nat. Chem. Biol.* **2**, 367–368.
- Waldron, K. J., and Robinson, N. J. (2009) How do bacterial cells ensure that metalloproteins get the correct metal? *Nat. Rev. Microbiol.* **7**, 25–35.
- Pennella, M. A., Arunkumar, A. I., and Giedroc, D. P. (2006) Individual metal ligands play distinct functional roles in the zinc sensor *Staphylococcus aureus* CzxR. *J. Mol. Biol.* **356**, 1124–1136.
- Giedroc, D. P., and Arunkumar, A. I. (2007) Metal sensor proteins: nature's metalloregulated allosteric switches. *Dalton Trans.*, 3107–3120.
- Dietze, E. C., Wang, R. W., Lu, A. Y. H., and Atkins, W. M. (1996) Ligand effects on the fluorescence properties of tyrosine-9 in alpha 1-1 glutathione S-transferase. *Biochemistry* **35**, 6745–6753.

BI900115W